Application of hybrid RANS/VMS modeling to massively separated flows and rotating machines

F.Miralles[1], B.Sauvage[3], S.Wornom[1], B.Koobus[1], A.Dervieux[2,3]

[1] IMAG, Université de Montpellier, France,
[2] Société LEMMA, Sophia-Antipolis, France
[3] INRIA Sophia-Antipolis, France

The 18th International Conference on Fluid Flow Technologies, Budapest,
2 september, 2022

Goal and overview

Goal

This work is motivated by the development of accurate and efficient tools for simulation of acoustic radiation generated by rotating machines

We focus this presentation on modeling issues

1. Hybrid approach
2. Discussion circular cylinder cases
3. Application on rotating frame

- Why massively separated flows and rotating machines ?

Figure – Helicopter blades application, wind turbines and taxi drone

Modeling of turbulent flow : RANS description (1)

- Compressible Reynolds Averaged Navier-Stokes Equations :

$$\frac{\partial W_h}{\partial t} + \nabla \cdot F_c(W_h) - \nabla \cdot F_d(W_h) = \tau(W_h) \quad (1)$$

- RANS $k-\varepsilon$ Goldberg[1] and $k-R$ of Zhang[2] ($R = \frac{k^2}{\varepsilon}$) closure term :

$$\tau^{k-\varepsilon}(W_h) = \left(\overbrace{0}^{\rho}, \overbrace{\mathbf{0}}^{\rho\mathbf{u}}, \overbrace{0}^{\rho E}, \overbrace{\tau : \nabla\mathbf{u} - \rho\varepsilon}^{\rho k}, \overbrace{(C_1\tau : \nabla\mathbf{u} - C_2\rho\varepsilon + E)T^{-1}}^{\rho\varepsilon} \right)$$

$$\tau^{k-R}(W_h) = \left(\overbrace{0}^{\rho}, \overbrace{\mathbf{0}}^{\rho\mathbf{u}}, \overbrace{0}^{\rho E}, \overbrace{\mu_t\mathfrak{S}^2 - \rho\frac{k^2}{R}}^{\rho k}, \overbrace{c_1 T_t\mu_t\mathfrak{S}^2 - \min\left(\rho c_2 k, \mu_t\frac{|\Omega|}{a_1}\right)}^{\rho R} \right)$$

1. U. Goldberg, O. Peroomian et S. Chakravarthy. "A wall-distance-free $k-\varepsilon$ model with Enhanced Near-Wall Treatment". In : *Journal of Fluids Engineering* 120 (1998), p. 457-462.

2. Y. Zhang, Md Mizanur Rahman et Gang Chen. "Development of k-R turbulence model for wall-bounded flows". In : *Aerospace Science and Technology* 98 (2020), p. 105681. issn : 1270-9638. doi : https://doi.org/10.1016/j.ast.2020.105681. url : https://www.sciencedirect.com/science/article/pii/S1270963819327282.

Modeling of turbulent flow : RANS description (2)

- RANS $k-\varepsilon$ Goldberg and $k-R$ closure term :

$$\tau^{k-\varepsilon}(W_h) = \left(\overbrace{0}^{\rho}, \overbrace{\mathbf{0}}^{\rho\mathbf{u}}, \overbrace{0}^{\rho E}, \overbrace{\tau : \nabla\mathbf{u} - \rho\varepsilon}^{\rho k}, \overbrace{(C_1 \tau : \nabla\mathbf{u} - C_2\rho\varepsilon + E)T^{-1}}^{\rho\varepsilon} \right)$$

$$\tau^{k-R}(W_h) = \left(\overbrace{0}^{\rho}, \overbrace{\mathbf{0}}^{\rho\mathbf{u}}, \overbrace{0}^{\rho E}, \overbrace{\mu_t\mathfrak{S}^2 - \rho\frac{k^2}{R}}^{\rho k}, \overbrace{c_1 T_t \mu_t \mathfrak{S}^2 - \min\left(\rho c_2 k, \mu_t \frac{|\Omega|}{a_1}\right)}^{\rho R} \right)$$

- DDES [3] closure term $\rho\varepsilon$ or $\rho\frac{k^2}{R}$ is replaced by $\rho\frac{k^{3/2}}{\mathfrak{l}_{dies}}$ where :

$$\mathfrak{l}_{ddes} = \frac{k^{\frac{3}{2}}}{\varepsilon} - f_{ddes}\max\left(0, \frac{k^{\frac{3}{2}}}{\varepsilon} - 0.65\Delta\right), \quad \begin{array}{rcl} f_{ddes} & = & 1 - \tanh((8r_d)^3), \\ r_d & = & \dfrac{\nu_t + \nu}{\kappa^2 y^2 \max(\sqrt{\nabla\mathbf{u}:\nabla\mathbf{u}}, 10^{-10})} \end{array}$$

3. P.Spalart et al. "A New Version of Detached-eddy Simulation, Resistant to Ambiguous Grid Densities". In : *Theoretical and Computational Fluid Dynamics* 20 (juil. 2006), p. 181-195. doi : 10.1007/s00162-006-0015-0.

Modeling of turbulent flow : RANS description (3)

- RANS Spalart-Allmaras[4] closure term :

$$\tau^{S.A}(W_h) = \left(\overbrace{0}^{\rho}, \overbrace{\mathbf{0}}^{\rho\mathbf{u}}, \overbrace{0}^{\rho E}, \overbrace{\rho c_b|\Omega| - c_{\omega 1} f_\omega \left(\frac{\nu}{d}\right)^2}^{\rho\nu} \right)$$

- DDES closure term d is replaced by l_{ddes} where :

$$l_{ddes} = \frac{k^{\frac{3}{2}}}{\varepsilon} - f_{ddes} \max\left(0, \frac{k^{\frac{3}{2}}}{\varepsilon} - 0.65\Delta\right), \quad \begin{aligned} f_{ddes} &= 1 - \tanh((8r_d)^3), \\ r_d &= \frac{\nu_t+\nu}{\kappa^2 y^2 \max(\sqrt{\nabla\mathbf{u}:\nabla\mathbf{u}}, 10^{-10})} \end{aligned}$$

4. P. SPALART et S. ALLMARAS. "A one-equation turbulence model for aerodynamic flows". In : *30th Aerospace Sciences Meeting and Exhibit*. doi : 10.2514/6.1992-439. eprint : https://arc.aiaa.org/doi/pdf/10.2514/6.1992-439. url : https://arc.aiaa.org/doi/abs/10.2514/6.1992-439.

LES component : Dynamic Variational Multi Scale

- VMS Principle

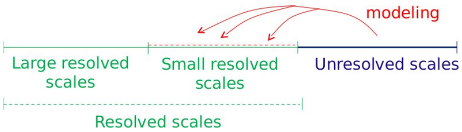

Our VMS [5] uses 2 embedded grids in order to dissipate solely the numerical scales which are the smallest represented by the mesh and not the larger ones.

- Dynamic VMS [6] is a combination of VMS with Germano-type dynamic algorithm adapting in space and time the SGS coefficient :

$$C_s \longrightarrow C_s(\mathbf{x}, t)$$

5. B.Koobus et C. Farhat. "A variational multiscale method for the large eddy simulation of compressible turbulent flows on unstructured meshes—application to vortex shedding". In : *Computer Methods in Applied Mechanics and Engineering* 193.15 (2004). Recent Advances in Stabilized and Multiscale Finite Element Methods, p. 1367-1383.

6. C. Moussaed et al. "Impact of dynamic subgrid-scale modeling in variational multiscale large-eddy simulation of bluff-body flows". In : *Acta Mechanica* 225 (2014), p. 3309-3323.

LES WALE vs VMS WALE

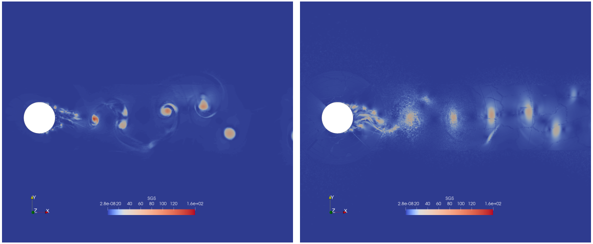

Figure – Flow past a circular cylinder at Re = 1M : SGS viscosity

Why Dynamic VMS ?

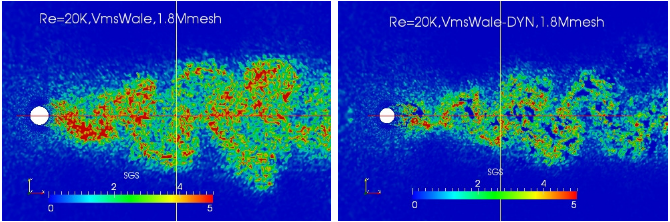

Figure – Flow past a circular cylinder at Re = 20K : SGS viscosity

- Hybrid description with finite volume/ finite element method

$$\left(\frac{\partial W_h}{\partial t}, \chi_i\right) + (\nabla \cdot F_c(W_h), \chi_i) = (\nabla \cdot F_d(W_h), \phi_i)$$

$$+ \theta \left(\tau^C(W_h), \phi_i\right) + (1-\theta)\left(\tau^{DVMS}(W_h^{small\ scales}), \phi_i^{small\ scales}\right)$$

- ⋆ $\tau^C \in \{\tau^{RANS}, \tau^{DDES}\}$
- ⋆ Blending : $\theta = 1 - f_d \times (1 - \overline{\theta})$; $\quad \overline{\theta} = \tanh\left(\left(\frac{\Delta}{k^{3/2}}\varepsilon\right)^2\right)$,
- ⋆ $f_d = f_{ddes}$

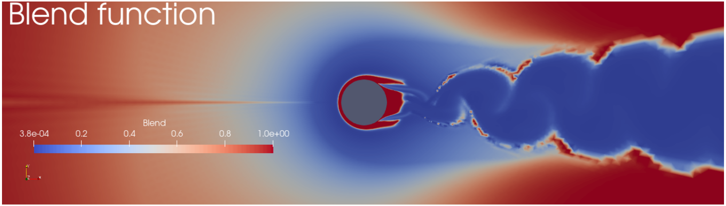

Figure – Hybrid RANS blending surface.

Set up

- Model used : RANS, DDES, VMS, RANS/DVMS, DDES/DVMS with :
  - Subgrid model for VMS : Smagorinsky, WALE
  - Closure model for RANS $k-\varepsilon$ of Goldberg, or $k-R$ or Spalart-Allmaras model.
- Simulation set up :
  - Mach number : 0.1 (subsonic flow)
  - reference pressure : 101300 $[\mathrm{N/m^2}]$
  - density : 1.225 $[\mathrm{kg/m^3}]$
  - Wall boundaries conditions :

$$\begin{aligned} \mathbf{u} = \mathbf{0}, &\quad \nabla E \cdot \mathbf{n} = 0,\ \nabla \rho \cdot \mathbf{n} = 0, \\ k-\varepsilon : &\quad k = 0,\ \varepsilon = (\nabla \sqrt{k}) \cdot \mathbf{n}, \\ \text{or } k-R : &\quad k = 0,\ R = 0, \\ \text{or } S.A : &\quad \nu_t = 0. \end{aligned}$$

  - The mesh is radial with minimal mesh size such that $y_w^+ \simeq 1$.

Circular cylinder Re=3900 : sub-critical regime

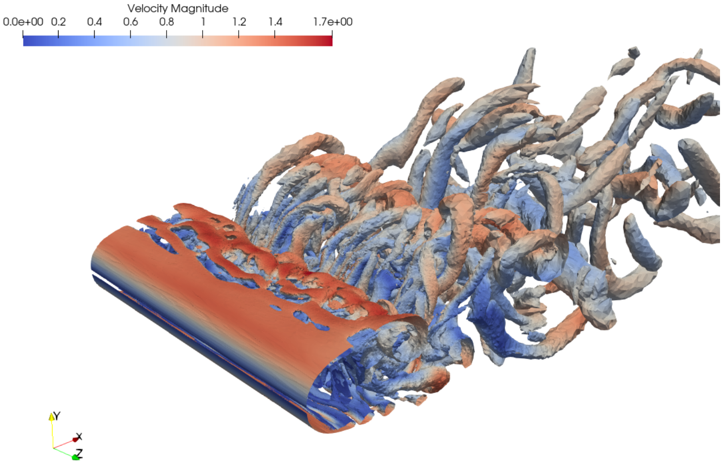

Figure – VMS-LES flow, Q-Criterion field using velocity color scale

Name	Mesh	δ_w	$\overline{C}_d$	C_l'	-C_{pb}	$\overline{\theta}$	St
Present simulation							
$k-\varepsilon$ Goldberg	176K	0.002	0.96	0.11	0.85	111	0.20
$k-R$	176K	0.002	1.00	0.11	0.86	93	0.20
DVMS WALE	1.46M	0.004	0.94	-	0.85	-	0.22
VMS	2.6M		0.99	0.11	0.88	89	0.21
VMS Adapted	230K		1.14	0.27	1.1	88	0.20
VMS Adapted	2.1M		1.06	0.18	1.00	85	0.20
Measurements							
Norberg [7] [8]	-	-	1.03	0.1	0.84	-	0.21
Kravchenko-Moin [9]	-	-	0.99	-	0.88	86	0.215

Table – Bulk coefficients of the flow around a circular cylinder at Reynolds number 3900, $\overline{C}_d$ holds for the mean drag coefficient, $\overline{C}_l'$ is the root mean square of lift time fluctuation, $\overline{C}_{p_b}$ is the pressure coefficient at cylinder basis, L_r is the mean recirculation length, $\overline{\theta}$ is the mean separation angle.

7. C Norberg. *Effects of Reynolds Number and Low-Intensity Freestream Turbulence on the Flow Around a Circular Cylinder*. Chalmers University of Technology, Gothenburg, Publikation Nr 87/2, mai 1987.

8. C Norberg. "Pressure Forces on a Circular Cylinder in Cross Flow, IUTAM Symposium on Bluff Body Wakes, Dynamics and Instabilities". In : sept. 1992. isbn : 978-3-662-00416-6.

9. A.Kravchenko et P. Moin. "Numerical studies of flow over a circular cylinder at ReD = 3900". In : *Physics of Fluids* 12 (fév. 2000). doi : 10.1063/1.870318.

■ Pressure coefficient and skin friction

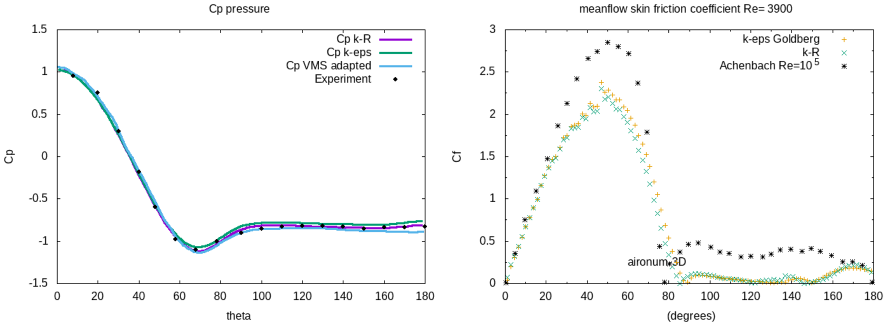

Figure – Distribution of mean pressure on left and skin friction on right side as a function of polar angle.

Circular cylinder Re = 1M : supercritical flow

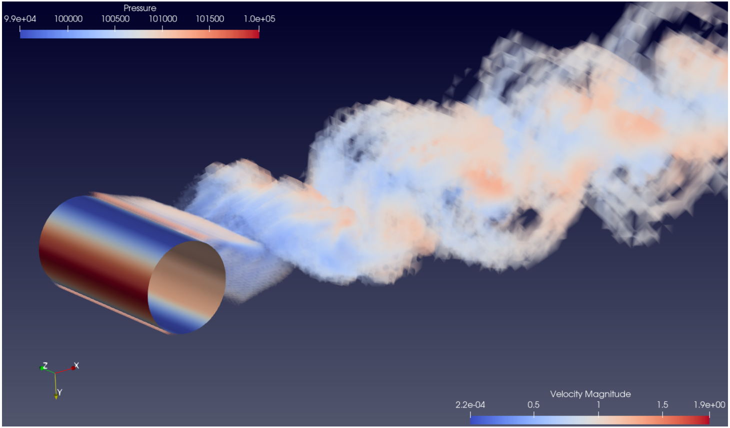

Figure – Hybrid URANS/DVMS, Q-Criterion field using velocity color scale

Pressure coefficient and skin friction

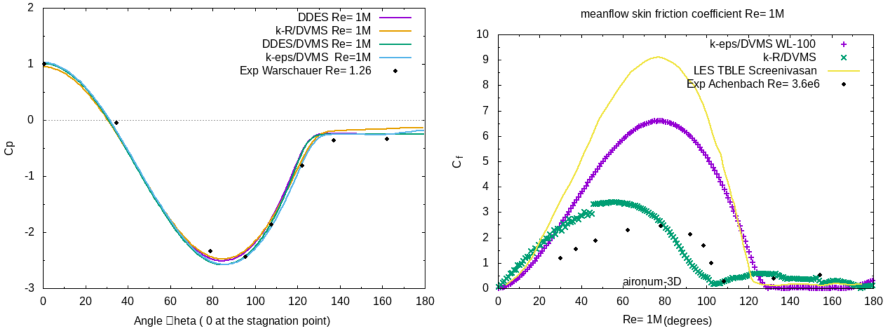

Figure – Distribution of mean pressure and mean skin friction coefficient as a function of polar angle.

Name	Mesh	y^+_{WL}	$\overline{C}_d$	C_l'	$-C_{pb}$	$\overline{\theta}$	St
Present simulation							
URANS $k-\varepsilon$	4.8M	0	0.50	0.24	0.61	109	0.46
DDES $k-\varepsilon$ WL	4.8M	100	0.20	0.04	0.22	138	0.18
DDES/ DVMS							
k - ε / WALE WL	4.8M	100	0.20	0.02	0.26	132	0.58
RANS / DVMS							
$k-R$ / DVMS WL	0.5M	10	0.18	0.02	0.14	135	0.56
k - ε / WALE WL	4.8M	100	0.26	0.11	0.22	134	0.42
Measurements							
Gölling [10]			0.24	-	-	130	0.48
Zdravkovich [11]			0.2-0.4	0.1-0.15	0.2-0.34	-	

Table – Bulk coefficients of the flow around a circular cylinder at Reynolds number 1M, $\overline{C}_d$ holds for the mean drag coefficient, C_l' is the root mean square of lift time fluctuation, $\overline{C}_{p_b}$ is the pressure coefficient at cylinder basis, L_r is the mean recirculation lenght, $\overline{\theta}$ is the mean separation angle.

10. B. Gölling. "Experimental investigations of separating boundary-layer flow from circular cylinder at Reynolds numbers from 105 up to 107". In : 2006, p. 455-462.

11. M.M. Zdravkovich. *Flow Around Circular Cylinders : Volume I : Fundamentals*. Flow Around Circular Cylinders : A Comprehensive Guide Through Flow Phenomena, Experiments, Applications, Mathematical Models, and Computer Simulations. OUP Oxford, 1997. isbn : 9780198563969. url : https://books.google.fr/books?id=w8tSQwAACAAJ.

Circular cylinder Re=2M : transcritical regime

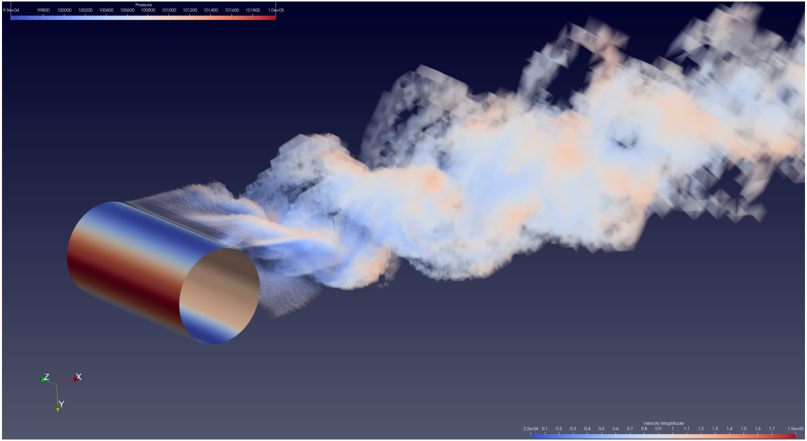

Figure – Hybrid URANS/DVMS with wall law, Q-Criterion field using velocity color scale

■ Pressure coefficient and skin friction

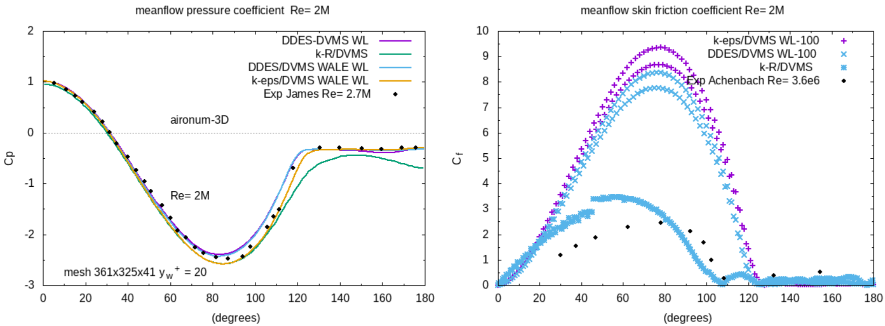

Figure – Distribution of mean pressure and skin friction coefficient as a function of polar angle.

	Mesh	y^+_{WL}	$\overline{C}_d$	C'_l	$-\overline{C_{pb}}$	$\overline{\theta}$	St
Present simulation							
URANS $k-\varepsilon$	4.8M	100	0.26	0.066	0.30	128	-
DDES $k-\varepsilon$ Goldberg	4.8M	100	0.28	0.038	0.27	132	-
DDES/ DVMS							
k - ε / Smagorinsky	4.8M	100	0.26	0.026	0.35	130	0.33
k - ε / WALE	4.8M	100	0.24	0.020	0.30	128	0.19
RANS / DVMS							
k - ε / Smagorinsky	4.8M	100	0.24	0.030	0.30	132	0.53
k - ε / WALE	4.8M	100	0.26	0.057	0.30	128	0.46
Other simul.							
LES/TBLE [12]			0.24	0.029	0.36	105	-
Measurements							
Exp. Shih [13]			0.26	0.033	0.40	105	
Exp. Schewe [14]			0.32	0.029	-		

Table – Bulk coefficients of the flow around a circular cylinder at Reynolds number 2×10^6.

12. A. Sreenivasan et B. Kannan. "Enhanced wall turbulence model for flow over cylinder at high Reynolds number". In : *AIP Advances* 095012 (2019).

13. W.C.L. Shih et al. "Experiments on flow past rough circular cylinders at large Reynolds numbers". In : *J. Wind Eng. Indust. Aerodyn.* 49 (1993), p. 351-368.

14. G. Schewe. "On the force fluctuations acting on a circular cylinder in crossflow from subcritical up to transcritical Reynolds numbers". In : *Journal of Fluid Mechanics* 133 (1995), p. 265-285.

Application on rotating frame : model presentation

- Set up of computation
  - NACA0012 at 6 angle of attack
  - Rotation speed : $\omega = 650 rpm$
  - tip $Mach = 0.22$

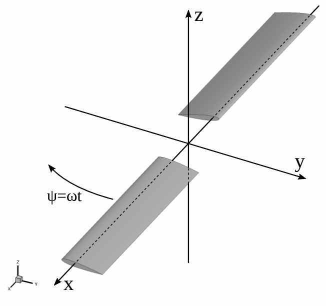

Simulation :

- RANS-SA adapted mesh (2.2M vertices)

(*)F. X. Caradonna, C. Tung, Technical Report NASA-TM-81232, 1981.

MRF method and mesh adaptation [15]

- Mesh adaptation

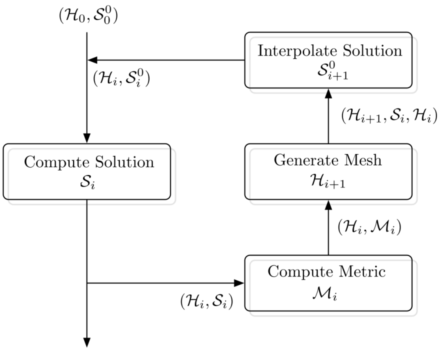

Figure – $\mathcal{H}$, $\mathcal{S}$ and $\mathcal{M}$ are respectively the mesh, the solution and the metric.

- Multiple Reference Frame (MRF)
  - Considering the velocity compositions :

$$\mathrm{u} = \mathrm{u}' + \boldsymbol{\omega} \times \boldsymbol{x}$$

    we rewrite the Navier-Stokes equations in absolute velocity formulation.
  - The computational domain is divided into two sub-domains. A cylindrical box around the helix where $|\boldsymbol{\omega}| = 650$ rpm, and an another cylindrical sub-domain around the box containing the helix where $|\boldsymbol{\omega}| = 0$.

15. F.Alauzet et al. "3D transient fixed point mesh adaptation for time-dependent problems : Application to CFD simulations". In : *J. Comput. Phys.* 222 (2007), p. 592-623.

Numerical results

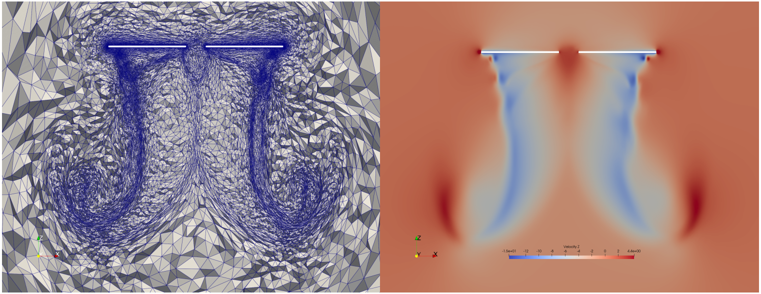

Figure – Caradonna-Tung simulation results : mesh (left) and velocity field (right) in cross-section.

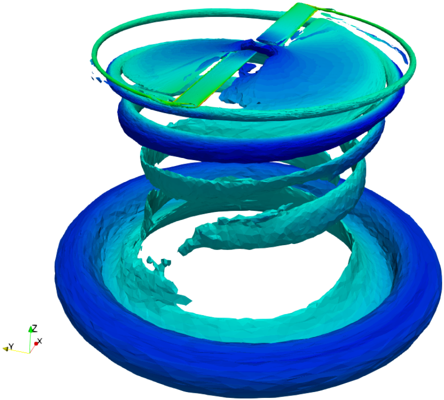

Figure – Caradonna-Tung simulation results : Q-criterion iso-surface.

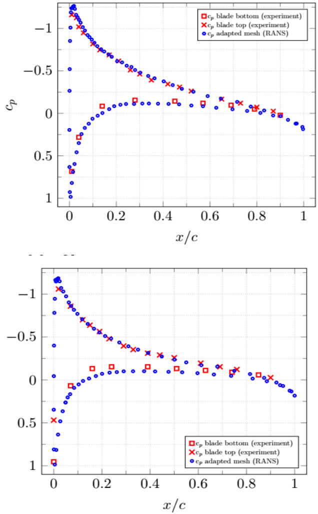

Figure – Pressure coefficient at $r/R = 0.89$ (left) and $r/R = 0.96$ (right) blade sections.

- Conclusion and perspective

  - Bulk coefficients are accurately predicted with hybrid approach
  - Hybrid models with wall law catch the separation of the flow
  - Rotation + RANS on adapted mesh give a correct shape of the results

- Use the adapted mesh for RANS/DVMS models
- Compute aeroacoustics using hybrid modeling

Appendix VMS

- VMS formulation [16]

$$\left(\frac{\partial W_h}{\partial t}, \chi_i\right) + (\nabla \cdot F_c(W_h), \chi_i) = (\nabla \cdot F_d(W_h), \phi_i) + \left(\tau^{DVMS}(W_h), \phi_i'\right) . \qquad (2)$$

- VMS closure term with dynamics coefficients $\mathcal{C}_{model} = \mathcal{C}_{model}(\mathbf{x}, t)$ and $Pr_t = Pr_t(\mathbf{x}, t)$

$$\left(\tau^{DVMS}(W_h), \phi_i'\right) = \left(0, \mathbf{M}_S(W_h, \phi_h'), M_H(W_h, \phi_h'), 0, 0\right)$$

where :

$$\begin{aligned} \mathbf{M}_S(W_h, \phi_i') &= \textstyle\sum_{T\in\Omega_h} \int_T \underbrace{\overline{\rho}(C_S\Delta)^2|S|}_{\mu_{sgs}} P\nabla\phi_i' d\mathbf{x}, \quad P = 2S - \tfrac{2}{3}Tr(S)Id \\ M_H(W_h, \phi_i') &= \textstyle\sum_{T\in\Omega_h} \int_T \frac{C_p}{Pr_t} \underbrace{\overline{\rho}(C_S\Delta)^2|S|}_{\mu_{sgs}} \nabla T' \cdot \nabla\phi_i' d\mathbf{x}, \quad \Delta = \left(\textstyle\int_T d\mathbf{x}\right)^{1/3} \end{aligned}$$

and $\phi_h' = \phi_h - \overline{\phi_h}$ where $\overline{\phi_h}$ is computed from macro cells.

16. C. Farhat, A. Rajasekharan et B. Koobus. "A dynamic variational multiscale method for large eddy simulations on unstructured meshes". In : *Computer Methods in Applied Mechanics and Engineering* 195.13 (2006). A Tribute to Thomas J.R. Hughes on the Occasion of his 60th Birthday, p. 1667-1691. issn : 0045-7825. doi : https://doi.org/10.1016/j.cma.2005.05.045. url : https://www.sciencedirect.com/science/article/pii/S0045782505003014.